JOURNAL OF ENVIRONMENTAL SCIENCES 100 (2021) 328–339

Available online at www.sciencedirect.com

ScienceDirect

www.elsevier.com/locate/jes

JES JOURNAL OF ENVIRONMENTAL SCIENCES

www.jesc.ac.cn

A theoretical study of hydrogen-bonded molecular clusters of sulfuric acid and organic acids with amides

Chenpeng Zuo[1,2], *Xianwei Zhao*[2], *Hetong Wang*[2], *Xiaohui Ma*[2], *Siyuan Zheng*[2], *Fei Xu*[1,2,*], *Qingzhu Zhang*[2]

[1] *Shenzhen Research Institute, Shandong University, Shenzhen 518057, China*
[2] *Environment Research Institute, Shandong University, Qingdao 266237, China*

ARTICLE INFO

Article history:
Received 14 August 2019
Revised 11 February 2020
Accepted 25 July 2020
Available online 16 August 2020

Keywords:
Amides
Sulfuric acid
Organic acids
Hydrogen bond
Nucleation

ABSTRACT

Amides, a series of significant atmospheric nitrogen-containing volatile organic compounds (VOCs), can participate in new particle formation (NPF) throught interacting with sulfuric acid (SA) and organic acids. In this study, we investigated the molecular interactions of formamide (FA), acetamide (AA), N-methylformamide (MF), propanamide (PA), N-methylacetamide (MA), and N,N-dimethylformamide (DMF) with SA, acetic acid (HAC), propanoic acid (PAC), oxalic acid (OA), and malonic acid (MOA). Global minimum of clusters were obtained through the association of the artificial bee colony (ABC) algorithm and density functional theory (DFT) calculations. The conformational analysis, thermochemical analysis, frequency analysis, and topological analysis were conducted to determine the interactions of hydrogen-bonded molecular clusters. The heterodimers formed a *hepta* or *octa* membered ring through four different types of hydrogen bonds, and the strength of the bonds are ranked in the following order: SO–H•••O > CO–H•••O > N–H•••O > C–H•••O. We also evaluated the stability of the clusters and found that the stabilization effect of amides with SA is weaker than that of amines with SA but stronger than that of ammonia (NH_3) with SA in the dimer formation of nucleation process. Additionally, the nucleation capacity of SA with amides is greater than that of organic acids with amides.

Introduction

Aerosols play a key role in the atmosphere system, which can influence the formation of cloud condensation nuclei (CNN), the earth radiation budget, photochemical reaction, and human health. The formation of new particles includes two stages: a nucleation stage where a metastable critical nucleus of about 1–3 nm in diameter is formed and a growth stage where the critical cluster increases easily (Kulmala et al., 2000). The nucleation process of gas phase species and continuous condensational growth in the atmosphere are significant.

Several mechanisms have been proposed to explain nucleation events in the troposphere, including binary SA/water (H_2O) nucleation, ternary SA/H_2O/NH_3 nucleation, ternary SA/H_2O/amines nucleation, ternary SA/H_2O/extremely low

* Corresponding author.
E-mail: xufei@sdu.edu.cn (F. Xu).

https://doi.org/10.1016/j.jes.2020.07.022
1001-0742/

volatile organic compounds (ELVOCs) nucleation, ion-mediated nucleation, iodine oxide nucleation and nucleation enhanced by organic compounds (Bianchi et al., 2016; Kumar et al., 2018a; Riccobono et al., 2014; Schobesberger et al., 2013; Sipila et al., 2016; Zhao et al., 2011). Sulfur dioxide (SO_2) is a global contaminant resulting from the combustion of sulfur-containing fossil fuels and volcanic eruption (Bao et al., 2010; Wark and Warner, 1998). SO_2 can be converted into sulfur trioxide (SO_3), SA, and sulfate through homogeneous and heterogeneous reactions (He and He, 2016; He et al., 2018). SA has been deemed as major atmospheric nucleation precursor (Zhang et al., 2011), but the atmospheric concentration of SA was unable to explain the field observed nucleation rate and growth rate of new particles (Yue et al., 2010). Consequently, SA should combine with stabilizing components such as ions, NH_3, amines, organic acids or highly oxidized multifunctional compounds (HOMs) to participate in the NPF (Ehn et al., 2014; Kulmala et al., 2013; Riccobono et al., 2014; Schobesberger et al., 2013; Xu and Zhang, 2012; Yu and Luo, 2014; Zhang et al., 2004). Organic acids, a series of important nucleation precursors, can promote atmospheric NPF. Zhang et al. found that the interaction between SA and aromatic acids contributes to efficient heterogeneous nucleation (Zhang et al., 2004). In addition, Zhang et al. reported that the interaction between SA and biogenic organic acids facilitates nucleation and primal growth of those particles (Zhang et al., 2009). Xu et al. pointed out that benzoic acid, maleic acid, tartaric acid, and phenylacetic acid are able to stabilize the small neutral clusters consisting of SA, and the stabilization efficiency of these substances seemingly are higher than or close to that of NH_3 (Xu et al., 2009). HAC is widely observed in the environment because it has a wide range of natural and anthropogenic sources and is closely related to human life. The stability of HAC with NH_3 is also found to be close to the stability of complexes of SA with NH_3 (Nadykto and Yu, 2007). HAC may efficiently stabilize small binary SA-H_2O clusters and interact actively with NH_3. OA and MOA are the richest species of dicarboxylic acids in the atmosphere and can accelerate the aerosol nucleation by binding with H_2SO_4 and NH_3 (Xu and Zhang, 2012).

Amides are a class of nitrogen-containing VOCs with a structural formula of R-CO–NR_2 (R = a hydrogen atom or an alkyl group). The amide bond (CO–N) is stable, neutral, and is able to accept or donate a hydrogen bond, which plays a crucial role in peptides, organic compounds, polymers, cosmetic products, and pharmaceuticals synthesis (Montalbetti and Falque, 2005). Amides are observed far and wide in the atmosphere and their primary emission sources include smoking, cooking, animal husbandry, combustion, sewage treatment, biomass burning, agriculture, and industrial production processes (Cheng et al., 2006; El Dib and Chakir, 2007; Ge et al., 2011; Kim et al., 2004; Kuhn et al., 2011; Leach et al., 1999; Nielsen et al., 2012; Schmeltz and Hoffmann, 1977; Zhu et al., 2013). Gaseous amides have been detected near the emission sources. The concentration of DMF is measured to exceed 4 ppbv near the waste and sewage operations (Leach et al., 1999). The concentration for AA reaches 4.21 g/kg from peat fires burning (Stockwell et al., 2016). Yao et al. (2016) conducted ambient measurements of amides in the urban area of Shanghai in China and found that concentrations of C_1 to C_6-amides were in the range of tens of pptv to a few ppbv, and the C_3-amides were most abundant amides and their concentration was up to 8.7 ppbv. In addition to the direct emission, amides are capable to be formed from the degradation routes of alkyl amines with OH and NO_3 radicals, Cl atom and O_3 molecule (Malloy et al., 2009; Murphy et al., 2007; Nielsen et al., 2012; Pitts et al., 1978; Tuazon et al., 1994). For example, ethanolamine (MEA) can react with OH radical and result in the formation of gaseous degradation products FA (Xie et al., 2014). The addition reaction of formamine with OH radical can form FA eventually (Borduas et al., 2016). Amides can also be produced through accretion reactions of carboxylic and dicarboxylic acids with NH_3 or amines. For example, acetic, malic, maleic, and pinic acid can transform into amides by atmospheric accretion reactions with NH_3 or amines (Barsanti and Pankow, 2006). Their atmospheric lifetime is dominated by particle formation, oxidation reactions, and deposition. Amides can also react with OH, NO_3, O_3, and Cl (Barnes et al., 2010; Borduas et al., 2014; El Dib and Chakir, 2007; Koch et al., 1997; Solignac et al., 2005) to lead to nitrogen-containing compounds formation which can promote the formation of secondary organic aerosol (SOA) (Barnes et al., 2010; Dahlin et al., 2008b; Roberts et al., 2011). Likewise, alkylamides can interact with atmospheric suspended SA particles in the presence of H_2O and contribute to the formation of ammonium and aminium salts (Barnes et al., 2010; Chen et al., 2017a; Dahlin et al., 2008a; Roberts et al., 2011). Although the formation and transformation reactions of amides in the atmosphere are widely studied, the exact contribution of amides during atmospheric nucleation and subsequent growth events is yet to be elucidated. For example, AA was found to only have a weaker enhancement capability on SA nucleation than amines (Dahlin et al., 2008a). However, Kumar et al. found that amides were inferred to play a vital role in NPF (Kumar et al., 2018b). In their study, urea was found to stabilize SA by forming the strongest hydrogen bonding complexes in comparison with formic, nitric, and methanesulfonic acid (Kumar et al., 2018b). In addition, amides are expected to interact with acids since they are prone to accept protons, which could compete with amines to react with acidic particles in places where concentrations of atmospheric amides are higher than those of amines (Chen et al., 2017a; Yao et al., 2016). Therefore, we should provide a more comprehensive knowledge of the role of amides in NPF and the characteristics of amide clusters.

In this study, DFT were carried out to study the molecular complexe formation between SA and organic acids with amides. Four organic acids are considered in this work, including HAC, PAC, OA, and MOA. In addition, we chose six alkylamides including FA, AA, MF, PA, MA, and DMF as the model compounds. Quantum chemical calculations were employed to determine the geometries and energetics of acids-amides dimers in this study. We also calculated the SO–H, CO–H, N–H, and C–H stretching frequencies of the donor monomer and their red or blue shifts upon formation of the complex. The red/blue shift is a typical feature of hydrogen bond formation. The quantum theory of atoms in molecules (AIM) was also analyzed to elucidate the nature of the hydrogen bonds of these complexes.

1. Materials and methods

1.1. Configurational sampling

In order to ensure the reliability of the configurational sampling, a systematic configurational sampling method and theoretical calculation are combined to search the global minima of clusters. To generate organic and inorganic molecular clusters, the ABC algorithm performed well in finding the minimum points on the potential energy surface (Karaboga, 2005). In the present paper, the initial configurations were produced by ABCluster software with the ABC algorithm (Zhang and Dolg, 2015, 2016). To ensure the accuracy, 1000 initial structures for every cluster would be generated and pre-optimized by the semi-empirical PM6 level (Stewart, 2007). After excluding the same and unreasonable structures, we selected 150 minimum energy configurations for subsequent optimization. The 150 structures selected were optimized by B3LYP functional at the 6–31 + G (d,p) basis set. The 30 minimum energy structures were selected again and further optimized by using the M06–2X functional at the 6–311 + G (2df, 2dp) basis set to obtain the global minimum.

1.2. Quantum chemical calculations

The DFT calculation was performed by Gaussian 09 (Revision A.01) software (Frisch et al., 2009). Geometry optimization and frequency calculations of molecular clusters were performed at the M06–2X/6–311+G (2df, 2dp) level of theory. The M06–2X density functional has been widely used and reproduced a great agreement with experimental and theoretical values of Gibbs free energy changes (ΔG) for SA-H_2O clusters (Shi et al., 2017). To ensure the accuracy of the M06–2X method, we compared the formation free energies of the SA-FA, SA-AA, SA-transMA clusters calculated at different methods. As listed in **Table S1**, the ΔG values at M06–2X/6–311+G (2df, 2dp) level are consistent with the results of CCSD(T)/cc-pvtz calculations. Thermodynamic properties including electronic energy, entropy, enthalpy, and Gibbs free energies were calculated using M06–2X method at the 6–311+G (2df, 2dp) basis set. The electronic energy of the complexes were corrected with zero point energy. Furthermore, structural characteristics and vibrational spectra were gained to analyze the properties of hydrogen bonds.

1.3. Topological analysis

The topological analysis was performed by using the AIM theory with the AIM2000 package at the M06–2X/6–311+G (2df, 2dp) level to investigate the nature of hydrogen-bonded complexes (Bader, 1990; Biegler-Konig et al., 2001; Biegler-Konig, 2000; Biegler-Konig and Schönbohm, 2002). We focused on the topological properties, such as change in atomic charge at the H atom, electron density and its Laplacian at bond critical points (BCPs), to assess the strength of hydrogen bond interactions between acids and amides.

2. Results and discussion

SA, HAC, PAC, OA, and MOA were selected as common atmospheric nucleation precursors. FA, AA, MF, PA, MA, and DMF, as a stabilizer, are added to the acids molecules. MF and MA have trans-structures and cis-structures according to the same or opposite directions of C=O and N–H bonds along the C–N axis. The theoretical calculation shows that the cis-structure is slightly more stable than trans-structure, which is consistent with previous study (Ma et al., 2019). For example, the electronic energy of cis-methylformamide (cis-MF) and cis-N-methylacetamide (cis-MA) is 1.20 and 1.77 kcal/mol lower than those of trans-methylformamide (trans-MF) and trans-N-methylacetamide (trans-MA) at the M06–2X/6–311+G (2df, 2dp) level. However, amides with trans-structure tend to be more stable than amides with cis-structure in the process of dimer formation. Thus, we choose trans-MF and trans-MA as representative (Ma et al., 2019).

2.1. Conformational analysis

The optimized configurations of the monomers of acids and amides at the M06–2X/6–311+G (2df, 2dp) level are shown in **Fig. S1**. We calculated optimized geometries of SA, HAC, PAC, OA, and MOA with FA, AA, trans-MF, PA, trans-MA, and DMF at the M06–2X/6–311+G (2df, 2dp) level. Molecular graphics generated by using Molden software package are shown in Fig. 1 (Schaftenaar and Noordik, 2000). Hydrogen bonding interaction is one of the driving forces for the formation of atmospheric molecular complexes. The strength of hydrogen bond determines the thermodynamic stability of the complexes. Four types of the hydrogen bond interaction were formed in the clusters of acids-amides. The first type is SO–H•••O bond formed by connecting the H atom in the SA and the carbonyl oxygen in the amides; the second type is CO–H•••O hydrogen bond between the H atom in the organic acids and the carbonyl oxygen in the amides;the third type is N–H•••O bond produced by connecting the H atom in amino of amides and the O atom in the acids;the fourth type is C–H•••O bond between the H atom on carbonyl carbon in the DMF and the O atom in the acids. FA, AA, trans-MF, PA, and trans-MA with five kinds of acids form an *octa* ring dimer with a SO–H•••O bond or CO–H•••O bond and a N–H•••O bond. Moreover, DMF with five kinds of acids form a *hepta* ring dimer with a SO–H•••O bond or CO–H•••O bond and a C–H•••O bond. The geometric parameters of SO–H•••O, CO–H•••O, N–H•••O, and C–H•••O hydrogen bond in binary acids-amides clusters are shown in Table 1.

Homonuclear hydrogen bond (O–H•••O) is called resonance-assisted hydrogen bonding where two oxygen atoms are inter-connected by a system of π-conjugated double bonds. The distance of two oxygen atoms d(O–O) in the hydrogen bond can be used as an indicator of hydrogen bonding strength. The distance is classified into extremely strong for d(O–O) < 2.5 Å, strong for 2.5 Å < d(O–O) < 2.65 Å, medium for 2.65 Å < d(O–O) < 2.8 Å and weak for d(O–O) > 2.8 Å (Gilli et al., 1994). As shown in Table 1, the interactions in SA-AA, SA-transMF, SA-PA, SA-transMA, and SA-DMF clusters belong to an extremely strong intermolecular hydrogen bonds because the distances d(O–O) are

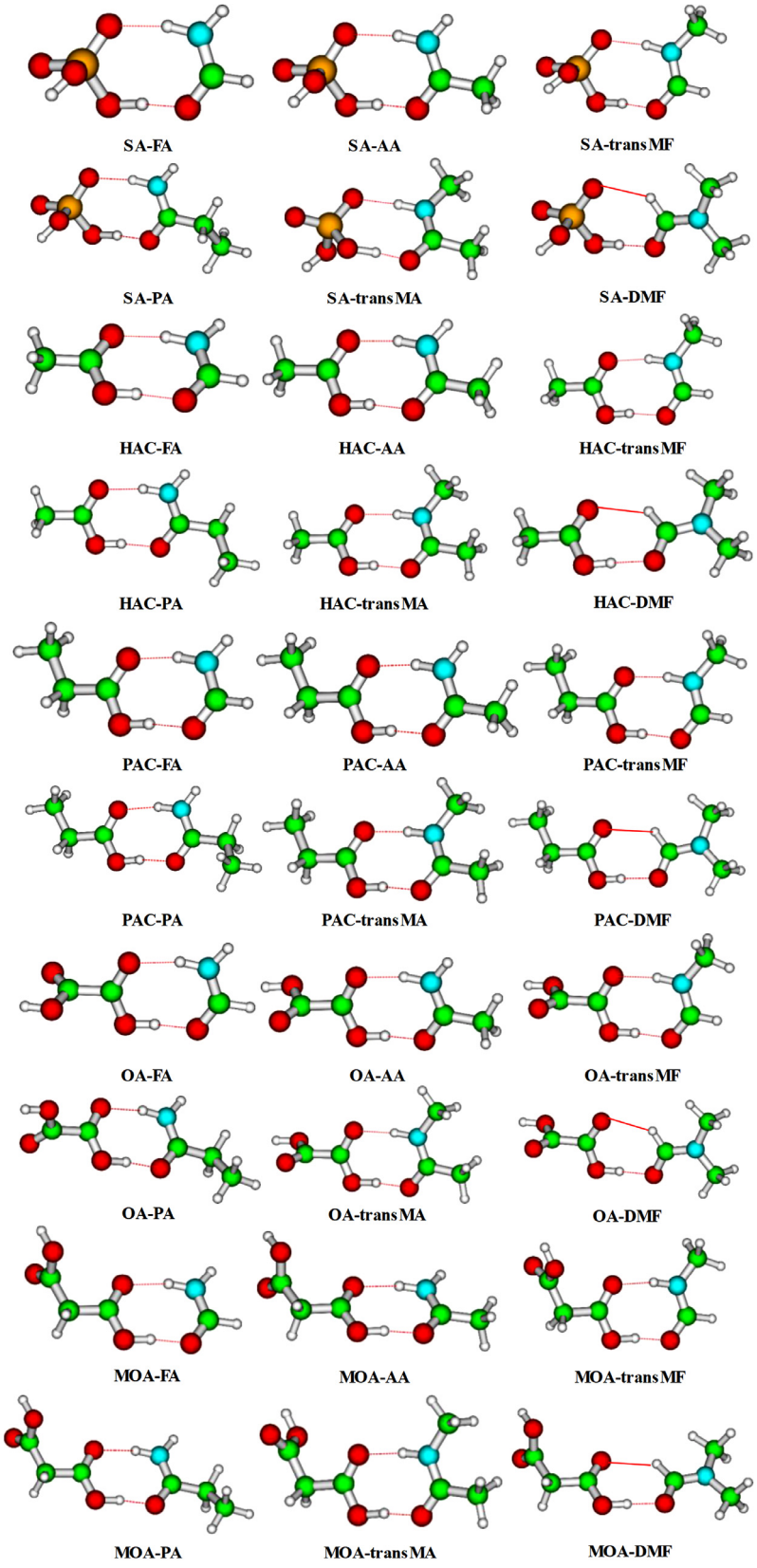

Fig. 1 – Optimized geometries of SA, HAC, PAC, OA, and MOA with FA, AA, trans-MF, PA, trans-MA and DMF calculated at M06–2X/6–311+G (2df, 2dp) level. Hydrogen bonds are indicated by red dashed lines. Color coding: blue = nitrogen, red = oxygen, white= hydrogen, green = carbon, orange = sulfur. (For interpretation of the references to color in this figure legend, the reader is referred to the web version of this article.)

Table 1 – Configuration parameters of SO–H···O, CO–H···O, N–H···O and C–H···O of the hydrogen bond in the clusters of acids-amides at the M06–2X/6–311+G(2df,2dp) level (length and distance in angstrom; angles in degree).

Dimers	SO–H···O/CO–H···O				N–H···O/C–H···O			
	Δr(OH)[a]	r(HB)[b]	θ(HB)[c]	d(O–O)[d]	Δr(NH/CH)[e]	r(HB)	θ(HB)	d(C/N–O)[f]
SA-FA	0.069	1.473	175.4	2.506	0.015	1.886	161.6	2.870
SA-AA	0.084	1.430	174.3	2.477	0.012	1.878	164.6	2.871
SA-transMF	0.008	1.439	175.0	2.483	0.012	1.880	166.2	2.881
SA-PA	0.082	1.435	174.6	2.480	0.012	1.888	163.8	2.879
SA-transMA	0.095	1.404	173.9	2.462	0.012	1.869	170.3	2.878
SA-DMF	0.073	1.459	179.2	2.498	–0.009	2.255	127.6	3.047
HAC-FA	0.034	1.636	175.4	2.634	0.015	1.863	163.1	2.855
HAC-AA	0.039	1.603	174.6	2.605	0.015	1.863	165.4	2.862
HAC-transMF	0.038	1.612	175.3	2.613	0.015	1.862	166.4	2.866
HAC-PA	0.037	1.610	174.8	2.611	0.017	1.875	164.6	2.871
HAC-transMFA	0.038	1.612	175.3	2.613	0.015	1.862	166.4	2.866
HAC-DMF	0.034	1.628	179.3	2.627	–0.007	2.267	128.5	3.071
PAC-FA	0.033	1.641	175.6	2.638	0.015	1.864	170.0	2.856
PAC-AA	0.038	1.610	175.0	2.611	0.015	1.864	165.1	2.862
PAC-transMF	0.037	1.615	175.4	2.616	0.014	1.865	166.3	2.869
PAC-PA	0.037	1.612	174.6	2.612	0.017	1.871	165.2	2.869
PAC-transMA	0.042	1.591	174.4	2.595	0.014	1.864	170.2	2.875
PAC-DMF	0.034	1.627	179.2	2.626	–0.007	2.266	128.4	3.070
OA-FA	0.047	1.564	176.4	2.575	0.012	1.901	160.5	2.882
OA-AA	0.052	1.536	175.3	2.553	0.012	1.905	163.3	2.895
OA-transMF	0.050	1.544	176.2	2.560	0.012	1.908	164.1	2.902
OA-PA	0.051	1.543	175.5	2.558	0.012	1.916	162.6	2.902
OA-transMA	0.057	1.521	175.0	2.542	0.012	1.900	168.3	2.904
OA-DMF	0.047	1.555	178.8	2.568	–0.009	2.301	127.2	3.088
MOA-FA	0.041	1.591	175.7	2.596	0.017	1.886	161.4	2.871
MOA-AA	0.047	1.560	174.8	2.571	0.014	1.883	164.0	2.876
MOA-transMF	0.046	1.567	175.6	2.577	0.013	1.884	164.9	2.882
MOA-PA	0.046	1.567	174.8	2.576	0.016	1.893	163.5	2.884
MOA-transMA	0.049	1.553	174.5	2.565	0.013	1.874	169.9	2.883
MOA-DMF	0.042	1.579	179.3	2.587	–0.007	2.282	127.8	3.078

[a] $\Delta r(OH) = r_{dimer} - r_{acid}$, is the change of length in the O–H bond upon complexation.
[b] Intermolecular hydrogen bond length.
[c] Intermolecular hydrogen bond angle.
[d] the distance between the two O atoms in the hydrogen bond (SO–H···O/CO–H···O).
[e] $\Delta r(NH/CH) = r_{dimer} - r_{amide}$, is the change of length in the N–H or C–H bond upon complexation.
[f] the distance between N/C and O atoms in the hydrogen bond (N–H···O/C–H···O).

less than 2.5 Å; the interactions in other clusters are strong intermolecular hydrogen bonds as the distances d(O–O) are in the range of 2.5–2.65 Å. The distances (r(HB)) between H and O atoms in N–H···O hydrogen bond vary from 1.862 Å to 1.916 Å, which are longer than that (r(HB)) in the range of 1.404–1.473 Å in the SO–H···O hydrogen bond and in the range of 1.521–1.641 Å in the CO–H···O hydrogen bond. This indicates that the SO–H···O and CO–H···O hydrogen bonds are generally stronger than the N–H···O hydrogen bonds. The resonance effect weakens the nucleophilicity of nitrogen atoms in amides. Moreover, the steric hindrance of methyl groups also affects the ability of N atoms in amides to accept protons. The distances (r(HB)) between H and O atoms in C–H···O hydrogen bond (within 2.255–2.301 Å) are longer than that (r(HB)) in SO–H···O, CO–H···O, and N–H···O hydrogen bond, which indicates the C–H···O hydrogen bond is weaker than SO–H···O, CO–H···O, and or N–H···O hydrogen bond. Therefore, for all clusters of acids-amides, the OH in the acids is easier to form hydrogen bond with carbonyl oxygen in the amides.

Proton transfer can occur in cluster formation, which may stabilize the clusters. Some of the clusters in the formation process may exhibit proton transfer from an acid (e.g., inorganic acids, organic acids) to a base (e.g., NH_3, amines, amides). The OH bond length in the SA monomer is 0.976 Å. After bonded with dimethylamine, the OH bond is elongated to 1.686 Å (increase 0.710 Å), which indicates the existence of transfer of proton from oxygen (SA) to nitrogen (DMA) (Xu and Zhang, 2013). In contrast, there is no proton transfer in clusters of benzoic acid with NH_3. In the case of benzoic acid-NH_3 complex, the O–H and N–H bonds are elongated by 0.04 and 0.01 Å, respectively, which vary slightly from the value of a free monomer (Zhao et al., 2009). In this study, the changes in the OH bond length of acids (Δr(OH) in Table 1) vary from 0.008 to 0.095 Å in the acids-amides dimers, and the changes in the NH bond length of amides (Δr(NH) in Table 1) are much smaller (0.012–0.017 Å) in the acids-amides. The relative small changes of the OH or NH bond upon complexation clearly reveal that there is no proton transfer in the hydrogen bonding interactions between acids and amides.

Table 2 – Changes in electronic energy ΔE, enthalpy ΔH, entropy ΔS, Gibbs free energy ΔG and average Gibbs free energy $\overline{\Delta G}$ calculated at M06–2X/6–311+G(2df,2dp) level of theory for SA, HAC, PAC, OA, MOA with a series of amides.

Reactions	ΔE (kcal/mol, 0 K)	ΔH (kcal/mol, 298.15 K)	ΔS (cal mol^{-1} K^{-1}, 298.15 K)	ΔG (kcal/mol, 298.15 K)	$\overline{\Delta G}$
SA + FA ⇔ SA-FA	–18.6	–19.0	–37.2	–7.9 (–8.01[a,b])	–9.0
SA + AA ⇔ SA-AA	–20.2	–19.9	–33.4	–9.9 (–9.90[a])	
SA + transMF ⇔ SA-transMF	–20.2	–20.3	–34.5	–10.0 (–9.84[a])	
SA + PA ⇔ SA-PA	–19.8	–20.1	–40.0	–8.1	
SA + transMA ⇔ SA-transMA	–21.2	–20.8	–33.1	–10.9 (–10.46[a])	
SA + DMF ⇔ SA-DMF	–17.7	–17.6	–34.4	–7.4 (–7.74[a])	
HAC + FA ⇔ HAC-FA	–14.4	–14.6	–36.2	–3.8	–4.0
HAC + AA ⇔ HAC-AA	–15.1	–14.7	–33.1	–4.8	
HAC + transMF ⇔ HAC-transMF	–15.4	–15.9	–40.1	–3.9	
HAC + PA ⇔ HAC-PA	–14.8	–15.0	–40.0	–3.0	
HAC + transMA ⇔ HAC-transMA	–15.8	–15.7	–35.8	–5.1	
HAC + DMF ⇔ HAC-DMF	–12.2	–11.8	–28.9	–3.2	
PAC + FA ⇔ PAC-FA	–15.4	–15.7	–38.4	–4.2	–4.3
PAC + AA ⇔ PAC-AA	–16.3	–16.4	–39.1	–4.8	
PAC + transMF ⇔ PAC-transMF	–16.7	–17.1	–40.8	–4.9	
PAC + PA ⇔ PAC-PA	–16.0	–16.1	–40.4	–4.1	
PAC + transMA ⇔ PAC-transMA	–16.5	–16.0	–34.9	–5.6	
PAC + DMF ⇔ PAC-DMF	–13.3	–13.5	–38.8	–1.9	
OA + FA ⇔ OA-FA	–15.2	–15.5	–35.1	–5.0	–5.7
OA + AA ⇔ OA-AA	–16.4	–16.1	–33.2	–6.2	
OA + transMF ⇔ OA-transMF	–16.5	–16.5	–36.4	–5.7	
OA + PA ⇔ OA-PA	–16.3	–16.4	–39.7	–4.6	
OA + transMA ⇔ OA-transMA	–17.3	–16.7	–30.6	–7.6	
OA + DMF ⇔ OA-DMF	–14.4	–14.0	–30.2	–5.0	
MOA + FA ⇔ MOA-FA	–15.5	–15.8	–39.4	–4.0	–4.3
MOA + AA ⇔ MOA-AA	–16.6	–16.2	–35.6	–5.6	
MOA + transMF ⇔ MOA-transMF	–16.4	–16.5	–39.6	–4.7	
MOA + PA ⇔ MOA-PA	–16.0	–16.2	–42.4	–3.6	
MOA + transMA ⇔ MOA-transMA	–16.5	–16.0	–33.8	–5.9	
MOA + DMF ⇔ MOA-DMF	–13.6	–13.4	–37.5	–2.2	

[a] reference (Ma et al., 2019),.
[b] reference (Ge et al., 2018).

2.2. *Thermochemical analysis*

The thermodynamic properties of SA, HAC, PAC, OA, and MOA with six kinds of amides were calculated at the M06–2X/6–311+G (2df, 2dp) level of theory. The changes of electronic energy (ΔE), enthalpies (ΔH), entropies (ΔS), Gibbs free energy (ΔG), and average Gibbs free energy ($\overline{\Delta G}$) are summarized in Table 2.

The $\overline{\Delta G}$ of interaction of SA, HAC, PAC, OA, and MOA with amides (–9.0, –4.0, –4.3, –5.7, and –4.3 kcal/mol), which means that the potential of to participate to form dimers is as follows: SA > OA > MOA ≈ PAC > HAC, and SA has stronger interaction with amides than four organic acids. Considering the ubiquity of SA and amides in the atmosphere, the interaction between SA and amides can play an important role in the nucleation of nanoparticles. The results of the changes in ΔG of reactions of SA with amides are compared with that of SA-amides clusters obtained previously at M06–2X/6–311++G (3df, 3pd) level (Ma et al., 2019). The Gibbs free energy changes of SA with FA, AA, transMF, transMA, and DMF in the present work are consistent with the previous reported results within 0.44 kcal/mol (Ma et al., 2019). The slight error between the results may arise from the difference of method and basis set. When amide molecules were added to SA molecule, the values of ΔG range from –10.9 to –7.4 kcal/mol. For the amide groups, we can deduce from the formation Gibbs free energies that the potential to participate in NPF is as follows: transMA > transMF > AA > PA> FA > DMF. In order to clarify the contribution of amides to the NPF, NH_3, methylamine (MAE), dimethylamine (DMA), and trimethylamine (TMA) were selected as the references. The formation Gibbs free energy in SA-NH_3 cluster by Xu et al., (2009) and Nadykto and Yu, (2007) are all –7.77 kcal/mol calculated at the PW91PW91/6–311++G (3df, 3pd) level. The formation Gibbs free energy of SA with MAE, DMA, and TMA are –11.03, –11.38, and –10.56 kcal/mol in the study by Nadykto et al. (Nadykto et al., 2011) calculated at the PW91PW91/6–311++G (3df, 3pd) level, respectively. The values of Gibbs free energy changes of dimer SA-NH_3, SA-MAE, SA-DMA, and SA-TMA are –6.64, –9.95, –13.66, and –15.26 kcal/mol in the study by Kurtén et al. calculated at the RI-CC2/aug-cc-pV(T + d)Z//RI-MP2/aug-cc-pV(D + d)Z level, respectively (Kurten et al., 2008). As may be seen from the comparison above, we can achieve the qualitative conclusion that the NPF capability of amides with SA is weaker than that of aliphatic amine with SA, but much higher than that NH_3 with SA.

The values of Gibbs free energy changes of complexation from four organic acids with amides are also presented in Table 2. The formation of binary HAC-AA and HAC-transMA

dimers is favorable thermodynamically. The Gibbs free energy changes associated with the formation of both HAC-AA and HAC-transMA is negative, thus, these complexes are thermodynamically stable. The average Gibbs free energy changes of reaction of HAC with amides are more negative by 1.65 kcal/mol compared with the formation Gibbs free energy of HAC–NH_3 at the PW91PW91/6–311++G (3df, 3pd) level in the study by Nadykto and Yu (Nadykto and Yu, 2007). The contrast leads us to conclude that the stability of HAC-amides is stronger than HAC–NH_3. In addition, the interaction of PAC with transMF (–4.9 kcal/mol) and transMA (–5.6 kcal/mol) is much stronger than that of PAC with DMF (–1.9 kcal/mol). The $\overline{\Delta G}$ of interaction of OA with amides is –5.7 kcal/mol. In contrast, the values of $\overline{\Delta G}$ of reaction of OA with amides are more negative by 1.54 kcal/mol compared with the formation Gibbs free energy of OA-DMA at the M06–2X/6–311+G (2d, 2p) level in the study by Chen et al., (2017b). The reaction capacity of OA with amides is 1.28 kcal/mol stronger than that with NH_3 at the PW91PW91/6–311++G (3df, 3pd) level in the study by Xu et al., (2010). Thus, it can be concluded that the stabilization effect of amides is stronger than that of DMA and NH_3. Moreover, the formation Gibbs free energy of MOA-AA and MOA-transMA are similar with the error within 0.3 kcal/mol, but make a large error within 3.4–3.7 kcal/mol when compared with that of MOA-DMF. The $\overline{\Delta G}$ of reaction of MOA with amides (–4.3 kcal/mol) is only positive by 0.19 kcal/mol compared with the ΔG of MOA-NH_3 (–4.49 kcal/mol) at the PW91PW91/6–311++G (3df, 3pd)//B3LYP/6–311++G (2d, 2p) level (Xu and Zhang, 2012). So, amides have the slightly weaker interaction with MOA. In conclusion, the maximum formation Gibbs free energy of interaction for trans-MA with SA, HAC, PAC, OA, and MOA is reached and the minimum formation Gibbs free energy for DMF with SA, PAC, and MOA is reached expect HAC-DMF and OA-DMF clusters. So trans-MA has the strongest interaction with acids and DMF has the weakest nucleation capacity in the series of amides. This is due to a stronger SO–H•••O or CO–H•••O hydrogen bond with a N–H•••O hydrogen bond is formed in the acids-transMA dimers, however, a weaker C–H•••O hydrogen bond along with a N–H•••O hydrogen bond is formed in the acids-DMF dimers.

Table 3 – Calculated bonded SO–H, CO–H, N–H and C–H stretching vibrational frequencies (ν), frequency shifts ($\Delta\nu$), calculated relative intensities (f_D/f_M) of the SA-amides, HAC-amides, PAC-amides, OA-amides and MOA-amides dimers at the M06–2X/6–311+G (2df, 2dp) level.

Dimers	SO–H/CO–H			N–H/C–H		
	ν (cm^{-1})	$\Delta\nu$ (cm^{-1})	f_D/f_M	ν(cm^{-1})	$\Delta\nu$(cm^{-1})	f_D/f_M
SA-FA	2563	1260	9.9	3430	332	8.4
SA-AA	2339	1484	11.5	3438	335	11.3
SA-transMF	2392	1432	10.6	3436	207	15.4
SA-PA	2377	1447	12.2	3452	321	11.3
SA-transMA	2205	1619	11.5	3443	211	16.1
SA-DMF	2504	1320	12.7	3146	−131	0.1
HAC-FA	3122	713	14.2	3385	377	13.3
HAC-AA	3027	808	21.9	3375	398	16.7
HAC-transMF	3036	798	18.2	3355	287	22.9
HAC-PA	3037	797	22.6	3394	379	16.3
HAC-transMA	2983	851	23.9	3398	256	22.1
HAC-DMF	3130	705	17.6	3140	−124	0.6
PAC-FA	3126	708	13.9	3377	385	14.0
PAC-AA	3039	795	21.5	3379	393	17.2
PAC-transMF	3080	754	9.2	3381	261	23.4
PAC-PA	3033	801	22.9	3389	383	17.5
PAC-transMA	2985	849	23.8	3382	272	23.1
PAC-DMF	3103	731	12.2	3082	−66	0.6
OA-FA	2921	912	9.1	3444	318	9.5
OA-AA	2828	1005	10.6	3428	344	12.7
OA-transMF	2856	977	9.8	3424	219	17.2
OA-PA	2846	987	11.0	3445	328	12.5
OA-transMA	2755	1078	11.3	3441	213	17.8
OA-DMF	2920	913	11.7	3115	−100	0.1
MOA-FA	2993	838	22.5	3407	355	11.4
MOA-AA	2885	946	26.6	3405	368	14.7
MOA-transMF	2924	906	24.5	3393	250	20.1
MOA-PA	2928	902	27.6	3423	349	14.8
MOA-transMA	2870	961	27.2	3410	245	20.7
MOA-DMF	2968	863	29.7	3134	−119	0.1

[a]the value of the SO–H, CO–H, N–H and C–H stretching vibrational frequencies of dimers.
[b]$\Delta\nu = \nu_{monomer} - \nu_{dimer,}$.
[c]f_D/f_M is on behalf of the intensity ratio of dimer to monomer.

2.3. *Frequency analysis*

Lengthening or shortening of the bonds in the monomer results in the red or blue shift of the stretching vibrational frequencies during the formation of the hydrogen bonds. The frequency shifts ($\Delta\nu$) of SO–H, CO–H, N–H, and C–H bonds between the monomer and dimer are useful to determine the relative strength of hydrogen bond interaction (Du and Kjaergaard, 2011; Tang et al., 2016; Zhang and Du, 2016; Zhao et al., 2016). The calculated SO–H, CO–H, N–H, and C–H stretching vibrational frequencies (ν), frequency shifts ($\Delta\nu$), and relative intensities (f_D/f_M) of complexation at the M06–2X/6–311+G (2df, 2dp) level are summarized in Table 3.

The elongation of the SO–H and N–H bonds in the SA-FA complex is 0.069 and 0.015 Å, respectively, which lead to red shifts of 1260 and 332 cm^{-1} of the corresponding stretching vibrational frequencies. For the SA-DMF complex, the SO–H bond length increased by 0.073 Å, corresponding to a red shift of 1320 cm^{-1}. The only blue shift of –131 cm^{-1} in the SA-DMF complex is 0.009 Å shortening of the C–H bond. This consistents with the typical feature for C–H•••O hydrogen bonds, which is the blue shifts of the C–H vibrational fundamental transitions with lower transition intensities in regard to the monomer (Delanoye et al., 2002; Lynch et al., 2018; Van der Veken et al., 2001). The red shifts of the SA-amides are significantly larger than those of organic acids-amides. The red shifts of SO–H and CO–H for the acids and amides complexes are in the region of 1260–1320 and 705–1078 cm^{-1}, respectively. The larger red shifts of complexes with SO–H•••O hydrogen bonds indicate stronger hydrogen bond than that with CO–H•••O hydrogen bonds, which is consistent with the conformational and thermochemical analysis above.

Infrared spectroscopy has been considered as one of the most important methods to investigate hydrogen bonding interactions. Infrared intensity increase is often observed for the hydrogen stretching vibration of a hydrogen bond donor and is often considered as a defining feature of a typical hydro-

Table 4 – AIM parameters for the SA-amides, HAC-amides, PAC-amides, OA-amides and MOA-amides dimers obtained at the M06–2X/6–311+G(2df,2dp) level. All values are in a.u.

Dimers	SO–H•••O/CO–H•••O			N–H•••O/C–H•••O		
	Δq(H)[a]	ρ(BCP)[b]	$\nabla^2\rho$(BCP)[c]	Δq(H)[a]	ρ(BCP)[b]	$\nabla^2\rho$(BCP)[c]
SA-FA	0.037	0.0881	0.0698	0.085	0.0340	0.1013
SA-AA	0.034	0.1017	0.0408	0.087	0.0352	0.1022
SA-transMF	0.034	0.0981	0.0497	0.087	0.0352	0.1025
SA-PA	0.034	0.1028	0.0379	0.086	0.0349	0.1017
SA-transMA	0.029	0.1165	–0.0101	0.088	0.0373	0.1041
SA-DMF	0.037	0.0848	0.0755	0.084	0.0127	0.0444
HAC-FA	0.051	0.0606	0.0949	0.092	0.0401	0.1011
HAC-AA	0.053	0.0656	0.0937	0.091	0.0398	0.1002
HAC-transMF	0.053	0.0643	0.0940	0.093	0.0403	0.1010
HAC-PA	0.054	0.0655	0.0936	0.091	0.0393	0.0999
HAC-transMA	0.053	0.0686	0.0922	0.089	0.0399	0.0998
HAC-DMF	0.048	0.0577	0.0967	0.084	0.0145	0.0470
PAC-FA	0.053	0.0598	0.0952	0.092	0.0398	0.1010
PAC-AA	0.053	0.0647	0.0940	0.091	0.0398	0.1006
PAC-transMF	0.054	0.0636	0.0944	0.092	0.0399	0.1009
PAC-PA	0.054	0.0648	0.0939	0.090	0.0390	0.0998
PAC-transMA	0.053	0.0677	0.0923	0.089	0.0401	0.1002
PAC-DMF	0.048	0.0573	0.0970	0.081	0.0141	0.0458
OA-FA	0.045	0.0731	0.0878	0.085	0.0357	0.0977
OA-AA	0.045	0.0803	0.0819	0.085	0.0361	0.0973
OA-transMF	0.045	0.0784	0.0835	0.085	0.0361	0.0973
OA-PA	0.043	0.0806	0.0814	0.084	0.0355	0.0968
OA-transMA	0.043	0.0855	0.0750	0.083	0.0368	0.0973
OA-DMF	0.040	0.0717	0.0893	0.080	0.0135	0.0437
MOA-FA	0.049	0.0665	0.0925	0.088	0.0376	0.0997
MOA-AA	0.051	0.0726	0.0895	0.089	0.0377	0.0991
MOA-transMF	0.050	0.0710	0.0903	0.089	0.0379	0.0997
MOA-PA	0.050	0.0726	0.0893	0.088	0.0373	0.0988
MOA-transMA	0.049	0.0764	0.0864	0.087	0.0381	0.0989
MOA-DMF	0.044	0.0644	0.0943	0.081	0.0137	0.0444

[a] The change in electronic charge at H atom.
[b] The electron density at the BCPs.
[c] The Laplacian of electron density at the BCPs.

gen bond. The intensity ratio between dimer and monomer are listed in Table 3. The f_D/f_M of C–H stretching transitions vary from 0.1 to 0.6. However, the f_D/f_M of N–H stretching transitions lie in the range of 8.4–23.4, which is significantly higher than the C–H values.

2.4. *Topological analysis*

Topological analysis were studied by using the theory of AIM, which provided a feasible way to assess the hydrogen bond strength (Lane et al., 2013; Parthasarathi et al., 2006). The AIM plots of the acids-amides complexes with BCPs, ring critical points (RCPs) and electron density paths are shown in Fig. 2 . The topological parameters, including the change in electronic charge at H atom (Δq(H)), the electron density at the BCPs (ρ(BCP)), and the Laplacian of electron density at the BCPs ($\nabla^2\rho$(BCP)) at the M06–2X/6–311+G (2df, 2dp) level are listed in Table 4.

On the basis of the standard put forward by Popelier, the electron density ρ(BCP) and its Laplacian $\nabla^2\rho$(BCP) at the BCPs are in the range of 0.002–0.040 and 0.014–0.139 a.u. for a hydrogen bond, respectively (Grabowski, 2004; Koch and Popelier, 1995). The ρ(BCP) at the BCPs for the SO–H•••O and CO–H•••O hydrogen bonds are in the ranges of 0.0848–0.1165 and 0.0573–0.0855 a.u., respectively. These values are higher than the upper limit value of the electron density standard (0.002–0.040 a.u.) for a hydrogen bond. The larger ρ(BCP) means the greater hydrogen bond strength. The results of ρ(BCP) indicate that the SO–H•••O hydrogen bond is substantially stronger than the CO–H•••O hydrogen bond. Comparison of values of ρ(BCP) of N–H•••O bond and C–H•••O bond suggests that the strength of hydrogen bond N–H•••O (0.0340–0.0403 a.u.) is quite greater than that of hydrogen bond C–H•••O (0.0127–0.0340 a.u.). Thus, according to the consequence of ρ(BCP), the strength of the four types of hydrogen bonds can be ranked as follows: SO–H•••O > CO–H•••O > N–H•••O > C–H•••O. Similarly, the Laplacian of the electron density $\nabla^2\rho$(BCP) of the dimers is in the ranges of 0.0379–0.0755 and 0.0750–0.0970 a.u. for the SO–H•••O and CO–H•••O hydrogen bonds, respectively, within the criteria range (0.014–0.139 a.u.).

2.5. *Atmospheric implication*

To explain the role of SA, organic acids and amides in the atmosphere, the mass-balance equation was used to evaluate the atmospheric implication. Take SA-PA cluster as an example, the [SA–PA] concentration was calculated by Eq. (1):

$$[\text{SA-PA}] = [\text{SA}] \times [\text{PA}]\, e^{-\frac{\Delta G}{RT}} \quad (1)$$

where, [SA–PA], [SA], and [PA] are the atmospheric concentrations of SA-PA, SA, and FA, respectively. ΔG is the formation Gibbs free energy of the SA-PA cluster, R is the molar gas constant in J/(mol•K), and T is the temperature in K.

Eq. (1) reveals that the concentration of the SA-PA cluster is related to the concentrations of SA and PA and the value of the formation Gibbs free energy for cluster formation. In this study, the concentration range of SA, NH_3, DMA, OA, and PA were 1.00×10^5–1.00×10^7, 2.46×10^9–2.46×10^{11}, 2.46×10^7–2.46×10^9, 2.46×10^{11}–2.46×10^{14} and 1.47×10^9–2.14×10^{11} molecule cm^{-3}, respectively (Chen et al., 2017b; Kurten et al., 2008; Lin et al., 2019; Yao et al., 2016). Using Eq. (1) together with Gibbs free energies for complexation given in Table 2 and the formation Gibbs free energy of SA-NH_3 and SA-DMA (Nadykto et al., 2015; Nadykto and Yu, 2007; Lin et al., 2019), we have calculated the concentration range of the clusters for SA-NH_3, SA-DMA, SA-PA, and OA-PA, and the values were 7.32×10^0–7.32×10^4, 1.74×10^1–1.74×10^5, 5.18×10^0–8.70×10^4, and 3.46×10^4–5.82×10^9, respectively. We found that the concentration of dimers increased greatly by several orders of magnitude with the concentration increasing of gas-phase atmospheric contaminants. For example, the concentration of SA-PA is lower than that of SA-DMA and simliar with that of SA-NH_3 by comparing the dimer concentrations. Besides, the concentration of OA-PA heterodimer is higher than that of SA-PA. Thus, we can conclude that amides likely play an important role in driving NPF in consideration of the high concentration of amides in the atmosphere.

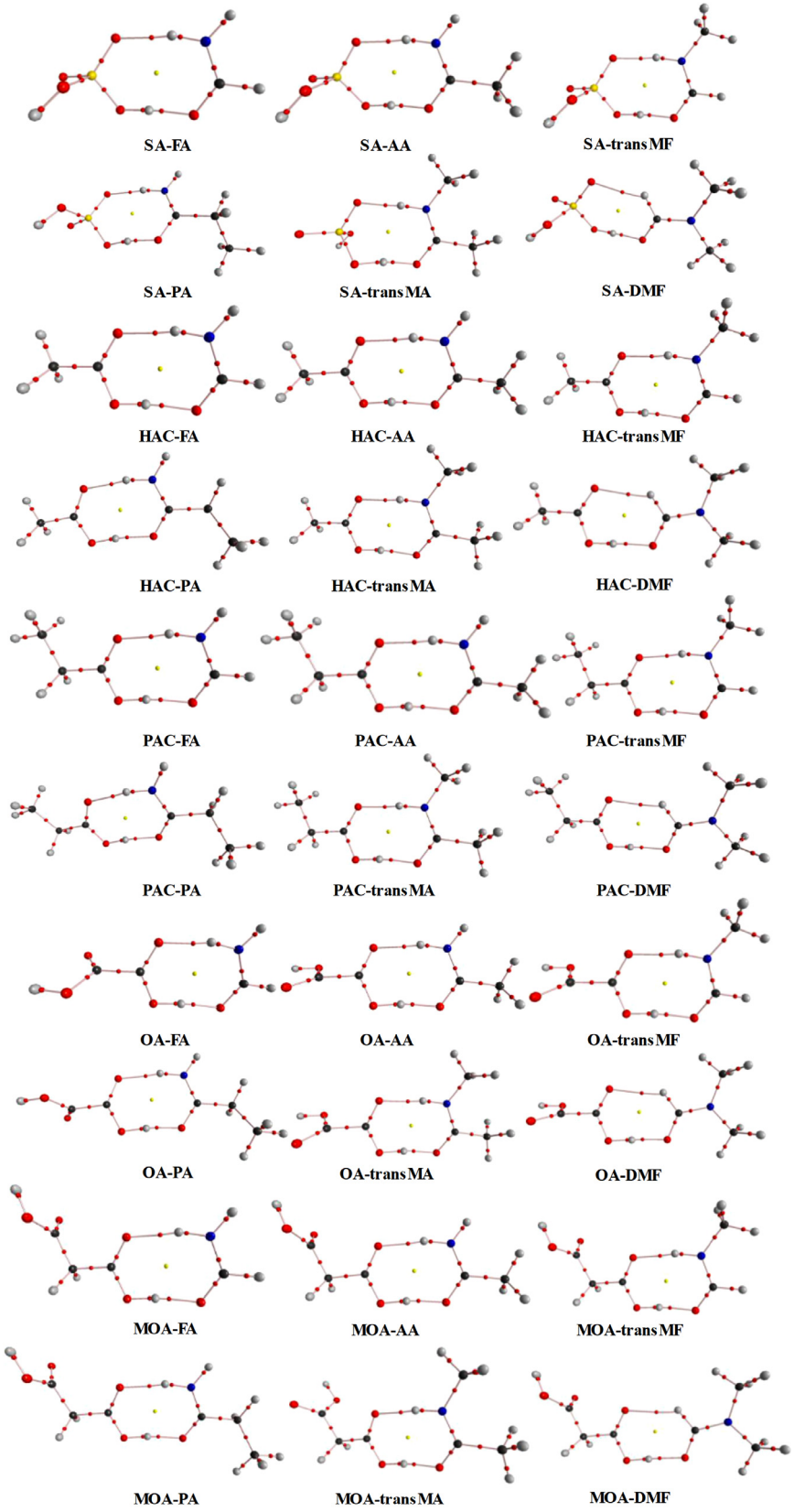

Fig. 2 – The AIM plots of SA, HAC, PAC, OA, and MOA with FA, AA, trans-MF, PA, trans-MA and DMF calculated at M06–2X/6–311+G(2df,2dp) level. The BCPs and RCPs are presented by the red and yellow nodes, respectively. (For interpretation of the references to color in this figure legend, the reader is referred to the web version of this article.)

3. Conclusions

In this study, we carried out quantum chemistry calculation to study the dimer formation from potential atmospheric nucleation precursors. The structures, energetics, frequencies and topologies of molecular complexes consisting of SA, organic acids with amides were investigated by using ABC algorithm and DFT theory. Three conclusions can be summarized as follows:

(1) The interaction between acids and amides leads to the formation of stable hydrogen bond complexes. The stabilization effect of amides with SA to form the dimers is weaker than that of amines with SA but stronger than that of NH_3 with SA. Among the six amides, trans-MA has the strongest stabilization effect and DMF has the weakest stabilization effect. Comparing the interaction between SA with amides and organic acids with amides, the nucleation capacity of SA with amides is stronger than that of organic acids with amides.
(2) By comparing the hydrogen bond length, vibration frequency and topological parameters, the strength of the four types of hydrogen bonds are ranked in the following order: SO–H•••O > CO–H•••O > N–H•••O > C–H•••O.
(3) Because amides are abundant in the atmosphere, strong hydrogen bond interaction between acids and amides provides the driving force for the acids-amides complexes formation. It is possible to reduce the nucleation barrier and promote the formation and growth of new particles by adding hydrophilic species (such as SA, H_2O, NH_3, etc.) to the hydrophilic side of clusters which can change the hydrophobicity of organic acids.

Acknowledgments

This work was supported by the National Natural Science Foundation of China (Nos. 91644214, 21677089, 21876102), the Shenzhen Science and Technology Research and Development Funds (No. JCYJ20160510165106371), the Fundamental Research Funds of Shandong University (Nos. 2016WLJH51, 2017JC033), The China Postdoctoral Science Foundation funded project (Nos. 2017M612277, 2017T100493), The open foundation of state key laboratory of environmental criteria and risk assessment, Chinese Research Academy of Environmental Sciences (Nos. 2016OFP09).

Appendix A Supplementary data

Supplementary material associated with this article can be found, in the online version, at doi:10.1016/j.jes.2020.07.022.

REFERENCES

Bader, R., 1990. Atoms in Molecules: a Quantum Theory. Clarendon Press, Oxford; New York.

Bao, H., Yu, S., Tong, D.Q., 2010. Massive volcanic SO_2 oxidation and sulphate aerosol deposition in Cenozoic North America. Nature 465, 909–912.

Barnes, I., Solignac, G., Mellouki, A., Becker, K.H., 2010. Aspects of the atmospheric chemistry of amides. Chem. Phys. Chem. 11, 3844–3857.

Barsanti, K.C., Pankow, J.F., 2006. Thermodynamics of the formation of atmospheric organic particulate matter by accretion reactions—Part 3: carboxylic and dicarboxylic acids. Atmos. Environ. 40, 6676–6686.

Bianchi, F., Trostl, J., Junninen, H., Frege, C., Henne, S., Hoyle, C.R., Molteni, U., Herrmann, E., Adamov, A., Bukowiecki, N., 2016. New particle formation in the free troposphere: a question of chemistry and timing. Science 352, 1109–1112.

Biegler-Konig, F., Schonbohm, J., Bayles, D., 2001. Software news and updates-AIM2000-a program to analyze and visualize atoms in molecules. J. Comput. Chem. 22, 545–559.

Biegler-Konig, F., 2000. Calculation of atomic integration data. J. Comput. Chem. 21, 1040–1048.

Biegler-Konig, F., Schonbohm, J., 2002. Update of the AIM2000-program for atoms in molecules. J. Comput. Chem. 23, 1489–1494.

Borduas, N., Abbatt, J.P., Murphy, J.G., So, S., da Silva, G., 2016. Gas-phase mechanisms of the reactions of reduced organic nitrogen compounds with OH radicals. Environ. Sci. Technol. 50, 11723–11734.

Borduas, N., da Silva, G., Murphy, J.G., Abbatt, J.P., 2014. Experimental and theoretical understanding of the gas phase oxidation of atmospheric amides with OH radicals: kinetics, products, and mechanisms. J. Phys. Chem. A 119, 4298–4308.

Chen, H., Wang, M., Yao, L., Chen, J., Wang, L., 2017a. Uptake of gaseous alkylamides by suspended sulfuric acid particles: formation of ammonium/aminium salts. Environ. Sci. Technol. 51, 11710–11717.

Chen, J., Jiang, S., Liu, Y.-.R., Huang, T., Wang, C.-.Y., Miao, S.-.K., Wang, Z.-.Q., Zhang, Y., Huang, W., 2017b. Interaction of oxalic acid with dimethylamine and its atmospheric implications. RSC Adv. 7, 6374–6388.

Cheng, Y., Li, S.-.M., Leithead, A., 2006. Chemical characteristics and origins of nitrogen-containing organic compounds in $PM_{2.5}$ aerosols in the Lower Fraser Valley. Environ. Sci. Technol. 40, 5846–5852.

Dahlin, J., Spanne, M., Dalene, M., Karlsson, D., Skarping, G., 2008a. Size-separated sampling and analysis of isocyanates in workplace aerosols—Part II: aging of aerosols from thermal degradation of polyurethane. Ann. Occup. Hyg. 52, 375–383.

Dahlin, J., Spanne, M., Karlsson, D., Dalene, M., Skarping, G., 2008b. Size-separated sampling and analysis of isocyanates in workplace aerosols. part I. denuder—Cascade impactor sampler. Ann. Occup. Hyg. 52, 361–374.

Delanoye, S.N., Herrebout, W.A., van der Veken, B.J., 2002. Blue shifting hydrogen bonding in the complexes of chlorofluoro haloforms with acetone-d_6 and oxirane-d_4. J. Am. Chem. Soc. 124, 11854–11855.

Du, L., Kjaergaard, H.G., 2011. Fourier transform infrared spectroscopy and theoretical study of dimethylamine dimer in the gas phase. J. Phys. Chem. A 115, 12097–12104.

Ehn, M., Thornton, J.A., Kleist, E., Sipila, M., Junninen, H., Pullinen, I., Springer, M., Rubach, F., Tillmann, R., Lee, B., 2014. A large source of low-volatility secondary organic aerosol. Nature 506, 476–479.

El Dib, G., Chakir, A., 2007. Temperature-dependence study of the gas-phase reactions of atmospheric NO_3 radicals with a series of amides. Atmos. Environ. 41, 5887–5896.

Frisch, M., Trucks, G., Schlegel, H.B., Scuseria, G., Robb, M., Cheeseman, J., Scalmani, G., Barone, V., Mennucci, B., Petersson, G., 2009. Gaussian 09, Revision A. 02. Gaussian, Inc, Wallingford, CT.

Ge, P., Luo, G., Luo, Y., Huang, W., Xie, H., Chen, J., 2018. A molecular-scale study on the hydration of sulfuric acid-amide complexes and the atmospheric implication. Chemosphere 213, 453–462.
Ge, X., Wexler, A.S., Clegg, S.L., 2011. Atmospheric amines–Part I. A review. Atmos. Environ. 45, 524–546.
Gilli, P., Bertolasi, V., Ferretti, V., Gilli, G., 1994. Covalent nature of the strong homonuclear hydrogen-bond-Study of the OH—O system by crystal-structure correlation methods. J. Am. Chem. Soc. 116, 909–915.
Grabowski, S.J., 2004. Hydrogen bonding strength—measures based on geometric and topological parameters. J. Phys. Org. Chem. 17, 18–31.
He, G., He, H., 2016. DFT studies on the heterogeneous oxidation of SO_2 by oxygen functional groups on graphene. Phys. Chem. Chem. Phys. 18, 31691–31697.
He, G., Ma, J., He, H., 2018. Role of carbonaceous aerosols in catalyzing sulfate formation. ACS Catal. 8, 3825–3832.
Karaboga, D., 2005. An idea based on honey bee swarm for numerical optimization.
Kim, H.A., Kim, K., Heo, Y., Lee, S.H., Choi, H.C., 2004. Biological monitoring of workers exposed to N,N-dimethylformamide in synthetic leather manufacturing factories in Korea. Int. Arch. Occup. Environ. Health 77, 108–112.
Koch, R., Palm, W.U., Zetzsch, C., 1997. First rate constants for reactions of OH radicals with amides. Int. J. Chem. Kinet. 29, 81–87.
Koch, U., Popelier, P.L., 1995. Characterization of CHO hydrogen bonds on the basis of the charge density. J. Phys. Chem. 99, 9747–9754.
Kuhn, U., Sintermann, J., Spirig, C., Jocher, M., Ammann, C., Neftel, A., 2011. Basic biogenic aerosol precursors: agricultural source attribution of volatile amines revised. Geophys. Res. Lett. 38, L16811.
Kulmala, M., Kontkanen, J., Junninen, H., Lehtipalo, K., Manninen, H.E., Nieminen, T., et al., 2013. Direct observations of atmospheric aerosol nucleation. Science 339, 943–946.
Kulmala, M., Pirjola, L., Makela, J.M., 2000. Stable sulphate clusters as a source of new atmospheric particles. Nature 404, 66–69.
Kumar, M., Saiz-Lopez, A., Francisco, J.S., 2018a. Single-molecule catalysis revealed: elucidating the mechanistic framework for the formation and growth of atmospheric iodine oxide aerosols in gas-phase and aqueous surface environments. J. Am. Chem. Soc. 140, 14704–14716.
Kumar, M., Trabelsi, T., Francisco, J.S., 2018b. Can urea be a seed for aerosol particle formation in air? J. Phys. Chem. A 122, 3261–3269.
Kurten, T., Loukonen, V., Vehkamaki, H., Kulmala, M., 2008. Amines are likely to enhance neutral and ion-induced sulfuric acid-water nucleation in the atmosphere more effectively than ammonia. Atmos. Chem. Phys. 8, 4095–4103.
Lane, J.R., Contreras-Garcia, J., Piquemal, J.-P., Miller, B.J., Kjaergaard, H.G., 2013. Are bond critical points really critical for hydrogen bonding? J. Chem. Theory Comput. 9, 3263–3266.
Leach, J., Blanch, A., Bianchi, A., 1999. Volatile organic compounds in an urban airborne environment adjacent to a municipal incinerator, waste collection centre and sewage treatment plant. Atmos. Environ. 33, 4309–4325.
Lin, Y., Ji, Y., Li, Y., Secrest, J., Xu, W., Xu, F., et al., 2019. Interaction between succinic acid and sulfuric acid–base clusters. Atmos. Chem. Phys. 19, 8003–8019.
Lynch, M.B., Lawrence, S.E., Nolan, M., 2018. Predicting nucleation of isonicotinamide from the solvent–solute interactions of isonicotinamide in common organic solvents. J. Phys. Chem. A 122, 3301–3312.
Ma, X., Sun, Y., Huang, Z., Zhang, Q., Wang, W., 2019. A density functional theory study of the molecular interactions between a series of amides and sulfuric acid. Chemosphere 214, 781–790.
Malloy, Q., Qi, L., Warren, B., Cocker Iii, D., Erupe, M., Silva, P., 2009. Secondary organic aerosol formation from primary aliphatic amines with NO_3 radical. Atmos. Chem. Phys. 9, 2051–2060.
Montalbetti, C.A., Falque, V., 2005. Amide bond formation and peptide coupling. Tetrahedron 61, 10827–10852.
Murphy, S., Sorooshian, A., Kroll, J., Ng, N., Chhabra, P., Tong, C., et al., 2007. Secondary aerosol formation from atmospheric reactions of aliphatic amines. Atmos. Chem. Phys. 7, 2313–2337.
Nadykto, A., Herb, J., Yu, F., Xu, Y., Nazarenko, E., 2015. Estimating the lower limit of the impact of amines on nucleation in the earth's atmosphere. Entropy 17, 2764–2780.
Nadykto, A., Yu, F., Jakovleva, M., Herb, J., Xu, Y., 2011. Amines in the earth's atmosphere: a density functional theory study of the thermochemistry of pre-nucleation clusters. Entropy 13, 554–569.
Nadykto, A.B., Yu, F., 2007. Strong hydrogen bonding between atmospheric nucleation precursors and common organics. Chem. Phys. Lett. 435, 14–18.
Nielsen, C.J., Herrmann, H., Weller, C., 2012. Atmospheric chemistry and environmental impact of the use of amines in carbon capture and storage (CCS). Chem. Soc. Rev. 41, 6684–6704.
Parthasarathi, R., Subramanian, V., Sathyamurthy, N., 2006. Hydrogen bonding without borders: an atoms-in-molecules perspective. J. Phys. Chem. A 110, 3349–3351.
Pitts Jr., J.N., Grosjean, D., Van Cauwenberghe, K., Schmid, J.P., Fitz, D.R., 1978. Photooxidation of aliphatic amines under simulated atmospheric conditions: formation of nitrosamines, nitramines, amides, and photochemical oxidant. Environ. Sci. Technol. 12, 946–953.
Riccobono, F., Schobesberger, S., Scott, C.E., Dommen, J., Ortega, I.K., Rondo, L., et al., 2014. Oxidation products of biogenic emissions contribute to nucleation of atmospheric particles. Science 344, 717–721.
Roberts, J.M., Veres, P.R., Cochran, A.K., Warneke, C., Burling, I.R., Yokelson, R.J., et al., 2011. Isocyanic acid in the atmosphere and its possible link to smoke-related health effects. Proc. Natl. Acad. Sci. 108, 8966–8971.
Schaftenaar, G., Noordik, J.H., 2000. Molden: a pre-and post-processing program for molecular and electronic structures. J. Comput.-Aided Mol. Des. 14, 123–134.
Schmeltz, I., Hoffmann, D., 1977. Nitrogen-containing compounds in tobacco and tobacco smoke. Chem. Rev. 77, 295–311.
Schobesberger, S., Junninen, H., Bianchi, F., Lönn, G., Ehn, M., Lehtipalo, K., et al., 2013. Molecular understanding of atmospheric particle formation from sulfuric acid and large oxidized organic molecules. Proc. Natl. Acad. Sci. 110, 17223–17228.
Shi, X.L., Zhang, R.M., Sun, Y.H., Xu, F., Zhang, Q.Z., Wang, W.X., 2017. A density functional theory study of aldehydes and their atmospheric products participating in nucleation. Phys. Chem. Chem. Phys. 20, 1005 -1001.
Sipila, M., Sarnela, N., Jokinen, T., Henschel, H., Junninen, H., Kontkanen, J., et al., 2016. Molecular-scale evidence of aerosol particle formation via sequential addition of HIO_3. Nature 537, 532–534.
Solignac, G., Mellouki, A., Le Bras, G., Barnes, I., Benter, T., 2005. Kinetics of the OH and Cl reactions with N-methylformamide, N,N-dimethylformamide and N,N-dimethylacetamide. J. Photochem. Photobiol., A 176, 136–142.
Stewart, J.J., 2007. Optimization of parameters for semiempirical methods V: modification of NDDO approximations and application to 70 elements. J. Mol. Model. 13, 1173–1213.
Stockwell, C.E., Jayarathne, T., Cochrane, M.A., Ryan, K.C., Putra, E.I., Saharjo, B.H., et al., 2016. Field measurements of trace gases and aerosols emitted by peat fires in Central Kalimantan, Indonesia, during the 2015 El Nino. Atmos. Chem. Phys. 16, 11711–11732.

Tang, S., Zhao, H., Du, L., 2016. Hydrogen bonding in alcohol–ethylene oxide and alcohol–ethylene sulfide complexes. RSC Adv. 6, 91233–91242.
Tuazon, E., Atkinson, R., Aschmann, S., Arey, J., 1994. Kinetics and products of the gas-phase reactions of O_3 with amines and related compounds. Res. Chem. Intermed. 20, 303–320.
Van der Veken, B.J., Herrebout, W.A., Szostak, R., Shchepkin, D.N., Havlas, Z., Hobza, P., 2001. The nature of improper, blue-shifting hydrogen bonding verified experimentally. J. Am. Chem. Soc. 123, 12290–12293.
Wark, K., Warner, C.F., 1998. Air pollution: Its Origin and Control. Addison-Wesley.
Xie, H.-.B., Li, C., He, N., Wang, C., Zhang, S., Chen, J., 2014. Atmospheric chemical reactions of monoethanolamine initiated by OH radical: mechanistic and kinetic study. Environ. Sci. Technol. 48, 1700–1706.
Xu, W., Zhang, R., 2012. Theoretical investigation of interaction of dicarboxylic acids with common aerosol nucleation precursors. J. Phys. Chem. A 116, 4539–4550.
Xu, W., Zhang, R., 2013. A theoretical study of hydrated molecular clusters of amines and dicarboxylic acids. J. Chem. Phys. 139, 064312.
Xu, Y., Nadykto, A.B., Yu, F., Herb, J., Wang, W., 2009. Interaction between common organic acids and trace nucleation species in the earth's atmosphere. J. Phys. Chem. A 114, 387–396.
Xu, Y., Nadykto, A.B., Yu, F., Jiang, L., Wang, W., 2010. Formation and properties of hydrogen-bonded complexes of common organic oxalic acid with atmospheric nucleation precursors. J. Mol. Struct. 951, 28–33.
Yao, L., Wang, M.-.Y., Wang, X.-.K., Liu, Y.-.J., Chen, H.-.F., Zheng, J., et al., 2016. Detection of atmospheric gaseous amines and amides by a high-resolution time-of-flight chemical ionization mass spectrometer with protonated ethanol reagent ions. Atmos. Chem. Phys. 16, 14527–14543.
Yu, F., Luo, G., 2014. Effect of solar variations on particle formation and cloud condensation nuclei. Environ. Res. Lett. 9, 045004.
Yue, D., Hu, M., Zhang, R., Wang, Z., Zheng, J., Wu, Z., et al., 2010. The roles of sulfuric acid in new particle formation and growth in the mega-city of Beijing. Atmos. Chem. Phys. 10, 4953–4960.
Zhang, J., Dolg, M., 2015. ABCluster: the artificial bee colony algorithm for cluster global optimization. Phys. Chem. Chem. Phys. 17, 24173–24181.
Zhang, J., Dolg, M., 2016. Global optimization of clusters of rigid molecules using the artificial bee colony algorithm. Phys. Chem. Chem. Phys. 18, 3003–3010.
Zhang, Q., Du, L., 2016. Hydrogen bonding in the carboxylic acid–aldehyde complexes. Comput. Theor. Chem. 1078, 123–128.
Zhang, R., Khalizov, A., Wang, L., Hu, M., Xu, W., 2011. Nucleation and growth of nanoparticles in the atmosphere. Chem. Rev. 112, 1957–2011.
Zhang, R., Suh, I., Zhao, J., Zhang, D., Fortner, E.C., Tie, X., et al., 2004. Atmospheric new particle formation enhanced by organic acids. Science 304, 1487–1490.
Zhao, H., Zhang, Q., Du, L., 2016. Hydrogen bonding in cyclic complexes of carboxylic acid–sulfuric acid and their atmospheric implications. RSC Adv. 6, 71733–71743.
Zhang, R., Wang, L., Khalizov, A.F., Zhao, J., Zheng, J., McGraw, R.L., et al., 2009. Formation of nanoparticles of blue haze enhanced by anthropogenic pollution. Proc. Natl. Acad. Sci. 106, 17650–17654.
Zhao, J., Khalizov, A., Zhang, R., McGraw, R., 2009. Hydrogen-bonding interaction in molecular complexes and clusters of aerosol nucleation precursors. J. Phys. Chem. A 113, 680–689.
Zhao, J., Smith, J., Eisele, F., Chen, M., Kuang, C., McMurry, P., 2011. Observation of neutral sulfuric acid-amine containing clusters in laboratory and ambient measurements. Atmos. Chem. Phys. 11, 10823–10836.
Zhu, L., Schade, G.W., Nielsen, C.J., 2013. Real-time monitoring of emissions from monoethanolamine-based industrial scale carbon capture facilities. Environ. Sci. Technol. 47, 14306–14314.